

Electronic structure, magnetic ordering, and optical properties of GaN and GaAs doped with MnE. Kulatov[†] and H. Nakayama**Department of Applied Physics, Faculty of Engineering, Osaka City University, 3-3-138 Sugimoto, Sumiyoshi, Osaka 558-8585, Japan*

H. Mariette

Laboratoire de Spectrometrie Physique, Universite J. Fourier, 17 avenue des Martyrs, 38054 Grenoble Cedex 9, France

H. Ohta

Department of Physics, Faculty of Science, Kobe University, 1-1 Rokkodai, Nada, Kobe 657-8501, Japan

Yu. A. Uspenskii

Tamm Theory Department, Lebedev Physical Institute, Russian Academy of Sciences, 117924 Leninskii prosp. 53, Moscow, Russia

(Received 23 March 2001; revised manuscript received 27 December 2001; published 22 July 2002)

The electronic structure and the properties of superdoped GaN(As):Mn (a concentration of Mn from 1.56% to 12.5%) are studied by using the tight-binding linear-muffin-tin-orbital method. Calculations show that the ferromagnetic state is lower in energy than the paramagnetic and antiferromagnetic states for both materials GaN:Mn and GaAs:Mn with all Mn concentrations. At the Fermi energy electronic states are 100% spin polarized, excluding GaAs:Mn with 12.5% of Mn. The most important difference between two materials concerns the energy position and localization of the Mn spin-majority states. In GaN these impurity states lie inside the fundamental gap and are well localized. In GaAs they are positioned near the top of the valence band and are strongly hybridized with it. This difference is clearly seen in the calculated magnetic, optical and, especially, kinetic properties of these materials, which are significantly different. Our investigation of codoping in GaN:Mn (substitution of O for N or Zn for Ga) shows that the atoms of O and Zn change the occupation of Mn bands and strongly affect both magnetic moments and conductivity.

DOI: 10.1103/PhysRevB.66.045203

PACS number(s): 71.15.Ap, 71.15.Rf, 75.50.Pp, 78.20.Ls

I. INTRODUCTION

Diluted magnetic semiconductors (DMS's) based on Mn-doped III-V and II-VI compounds have received extensive attention because of the physical interest in both so-called carrier-induced ferromagnetism and spin-electronics applications. Much current debate focuses on $\text{Ga}_{1-x}\text{Mn}_x\text{As}$. Using low-temperature molecular-beam-epitaxy techniques, Mn was incorporated into epitaxial layers of GaAs with concentrations x up to 0.07 (3.5% of Mn), which are beyond its solubility limit.¹ The magnetic impurity atom of Mn in GaAs, which occupies the cation (Ga) sublattice in the zincblende crystal structure, acts both as a source of localized spins and as an acceptor providing carriers (holes). For concentrations above $x=0.05$ (2.5% of Mn) GaAs:Mn has been reported as a ferromagnet with $T_c \approx 100$ K.² The origin of ferromagnetism in this DMS is still open to question.

From the standpoint of technology, superdoping (here doping beyond 1%) is relatively easy only in the case of "soft" semiconductors like GaAs, InAs, or CdTe. This is not the case with "hard" semiconductors like GaN or AlN. These materials need relatively high growth temperatures to obtain good crystalline quality. At such high temperatures superdoped transition-metal impurities cause segregation or form a compound with the host semiconductor elements. In order to obtain an extremely heavy doping of Mn, a highly nonequilibrium growth process is necessary. That is why less attention was paid to magnetically doped GaN:(3d-transition-metal) systems, although this class of DMS has been predicted to be ferromagnetic at room temperature.³

GaN-based DMS's are quite promising for various spin-controlled and photonic devices because of the wide gap corresponding to visible light. Another attractive property of GaN:Mn is its half-metallic ferromagnetism, that is, a 100% spin polarization of carriers at the Fermi energy. This provides an opportunity to overcome the intrinsic difficulty of injecting spins into a nonmagnetic semiconductor. Recently, a similar injection and evidence of spin-polarized current in III-V semiconductor has been demonstrated and a large signal from half-metallic DMS's was predicted.⁴ The growth of superdoped GaN:Mn using an ultrahigh-vacuum chemical vapor description system was reported in our work.⁵ In that study superconducting quantum interference device (SQUID) magnetization measurements showed the magnetic hysteresis at room temperature, i.e., the existence of room temperature ferromagnetism in granular GaN:Mn.⁶ Moreover Curie temperatures for the epitaxial wurtzite GaN:Mn films were also recently reported as high as 940 K (Ref. 7) (deduced from extrapolating SQUID measurements) and around room temperature⁸ (from the anomalous Hall effect).

These experimental results give a strong impetus to band-structure studies of superdoped GaN:Mn. A quantitative understanding of the properties of a material, especially the electronic states induced by a transition-metal dopant, is a clue to the material design of a class of magnetic semiconductors. Recently, we made band-structure calculations of superdoped Si:Mn.⁹ The results showed that the ferromagnetic state is the ground state of Si:Mn, regardless of whether substitutional or interstitial doping is considered. *Ab initio* studies of GaAs:Mn were made in Refs. 10–12 and 13–17.

Despite the different techniques used, all calculations showed that ferromagnetic state provides a significant gain in energy. It was also found that the filled spin-up (majority) bands of Mn are located near the top of the valence band (VB), while the empty spin-down (minority) bands of Mn are placed near the bottom of the conduction band (CB). Effects of the clustering of Mn atoms and their magnetic interaction were analyzed for GaAs:*M*, GaN:*M*, and AlN:*M* (*M* = Cr, Mn, or Fe) in the work.¹⁴

This paper focuses on an *ab initio* study of a zinc-blende GaN:Mn system in a range of Mn concentrations from 1.56% to 12.5%. In addition to the electronic structure, the magnetic, kinetic and optical properties of this system are calculated. To better understand the specifics of GaN:Mn, the same calculations are performed for GaAs:Mn. The results show a great difference between the properties of GaN:Mn and GaAs:Mn, which is caused by different energy positions of Mn states in the fundamental gaps of GaN and GaAs. The paper is organized as follows. Section II describes our theoretical approach. The electronic structures and magnetic properties of GaN:Mn and GaAs:Mn are considered and compared in Sec. III. An analysis and a comparison of the kinetic and optical properties of GaN:Mn and GaAs:Mn are given in Sec. IV. In view of a significant interest in the codoped DMS, the effect of substitution of O for N or Zn for Ga on properties of GaN:Mn is analyzed (Sec. V). The obtained results are summarized and discussed in Sec. VI.

II. METHOD OF CALCULATION

Our electronic structure calculations of GaN(As):Mn were performed by using the tight-binding linear-muffin-tin-orbital (TB-LMTO) method.¹⁸ The doping of Mn in GaN(As) can be modeled by means of a cubic supercell containing 64 atoms and 64 empty spheres (because the zinc-blende structure is open), in which one, two, four, and eight atoms of Ga are replaced by Mn atoms to simulate a uniformly doped semiconductor with 1.56%, 3.125%, 6.25%, and 12.5% Mn concentrations, respectively. To study the magnetic interactions between the Mn atoms, we constructed cubic 64-(2×2×2 in units of the zinc-blende lattice spacing a_0), tetragonal 32-($\sqrt{2}\times\sqrt{2}\times 2$), and tetragonal 16-($\sqrt{2}\times\sqrt{2}\times 1$) atom supercells with two Mn atoms. As a result, we obtain 3.125%, 6.25% and 12.5% Mn concentrations, respectively. The total energies of the paramagnetic (PM), ferromagnetic (FM), and antiferromagnetic (AFM) states have been calculated in these supercells, where the Mn atoms are separated as far as possible, i.e., two Mn atoms occupy the corner and the center of unit cell.

All calculations were made in the atomic sphere approximation with the combined correction terms. The ratio of atomic sphere radii can be determined from the interatomic minima of electron density calculated by using the full potential method. With this aim in view, we carried out a full potential LMTO (Ref. 19) calculation of GaN(As):Mn with 12.5% Mn. It was found that the densities of states (DOS's) and the electron and spin densities calculated by using this method and the TB-LMTO method with the "optimized" radii are practically identical. The obtained ratios of the radii

were then used in GaN(As):Mn at all Mn concentrations. For all calculations we assumed GaN and GaAs experimental lattice spacings of $a_0 = 8.504a_B$ and $10.677a_B$, respectively.

The TB-LMTO basis set consisted of 4*s*, 4*p*, and 3*d* orbitals of Mn, 4*s*, 4*p*, and 3*d* orbitals of Ga, and 2*s* (4*s*) and 2*p* (4*p*-) orbitals of N (As). For empty spheres only the 1*s* and 2*p* LMTO's were used. As for the interstitial 3*d*- and N (As) 3*d* (4*d*) partial waves, they were included only in LMTO tails. All **k**-space integrations were performed by using the tetrahedron method.²⁰ Convergence to self-consistency was achieved on the mesh of 119 **k** points in $\frac{1}{24}$ of the Brillouin zone, and checked through the total energy, which was stable within 10^{-6} Ry at the last few iterations. To calculate the DOS, the charge density maps, and kinetic and optical properties, a finer mesh of 451 **k** points was used.

The calculations showed that at all Mn concentrations, the DOS, and the electron and spin densities of GaN(As):Mn are rather insensitive to variation of the sphere radii within $\pm 10\%$ from the optimum. As an additional test of the calculational procedure, we compared our TB-LMTO electronic structure of the ferromagnetic GaAs:Mn containing 6.25% of Mn with the results of the full-potential linear-augmented-plane-wave calculations.^{12,15} The comparison shows that the two methods yield very similar results for the electronic structures. This confirms that the fast TB-LMTO method is accurate enough to study the electronic structure of DMS's with zinc-blende lattices in cases where the optimized sphere radii are used.

Exchange and correlation effects were included through the von Barth–Hedin local-spin-density approximation (LSDA).²¹ This point requires special consideration as the width of Mn bands is about 0.3–1.0 eV depending on the concentration. In our view, a strong argument to use the LSDA in this case is the observed metallic conductivity of GaAs:Mn.² This indicates that Mn states are collective enough to reduce strong electronic correlations, which are typical for narrow bands. Another argument is good agreement between the experimental energy of the Mn level in GaAs and the position of the Mn spin-up t_{2g} state calculated by using the LSDA.¹⁴ These arguments support the use of the local-density functionals for DMS's, though additional experimental verification of this point would be desirable.

III. ELECTRONIC STRUCTURES AND MAGNETIC PROPERTIES OF GaN(As) DOPED WITH Mn

The electronic structure of GaN:Mn with a 3.125% Mn concentration is of special interest because it corresponds to a typical value of Mn concentration usually obtained experimentally in III-V semiconductors. The calculated DOS and partial DOS's of this ferromagnetic DMS are presented in Fig. 1(a). The Mn impurity states placed in the gap region are of particular interest. These states are splitted by both exchange interaction $\Delta E_{xc} \equiv E(C_d^\downarrow) - E(C_d^\uparrow) \sim 3.4$ eV and crystal field $\Delta E_{\text{cryst}} \equiv E_{t_{2g}} - E_{e_g} \sim 1.35$ eV, where C_d^σ is the center of *d* band in the corresponding spin channel. In comparison with Ga, Mn has extra four valence electrons, which fill spin-up e_g and t_{2g} bands. The doubly degenerated e_g band is fully occupied, while the triply degenerated t_{2g} band

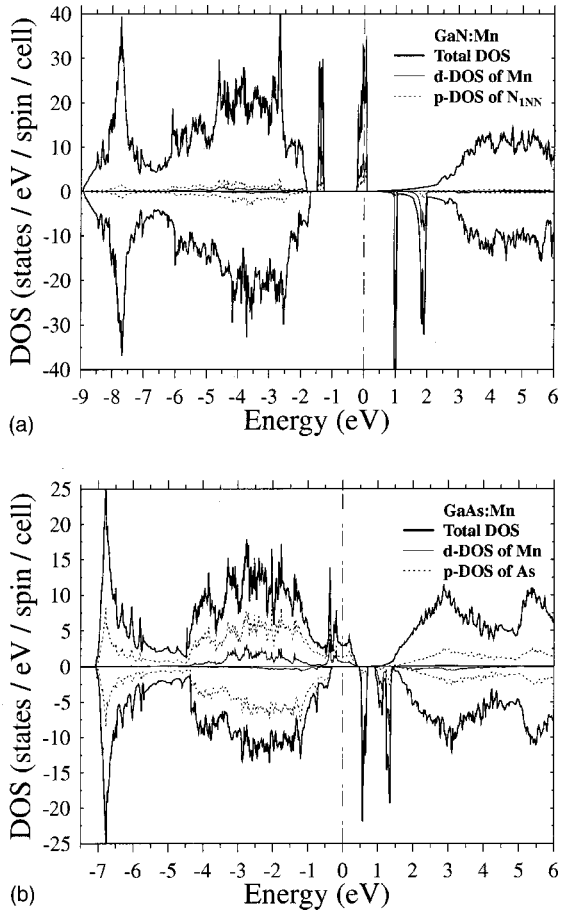


FIG. 1. Total and local partial densities of states in the ferromagnetic state of GaN: Mn (a) and GaAs:Mn (b) at 3.125% of Mn. Total DOS's are shown by bold lines, thin lines are the d DOS's of Mn, and dashed lines are the p DOS's of N (first-nearest neighbors, 1 NN) (a) and p DOS's of As (b). The vertical dot-dashed line denotes the position of the Fermi level which is set as zero energy.

(higher in energy) is only two-thirds filled so the Fermi level falls just into the latter 100% spin-polarized band [Fig. 2(a)]. As a result, the total magnetic moment has an integer value $M^{\text{total}} = 8\mu_B$. Moreover, our results show that the main part of this magnetic moment is strongly localized on the Mn site (Table I). The additional contributions to the total magnetic moment appear to come from N and Ga atoms in first nearest neighbors to Mn.

An important point is that the spin-up $3d$ states of Mn are located deeply inside the gap and therefore are weakly mixed with the VB and CB of GaN. This dictates a short-range character of impurity orbitals, the narrow e_g and t_{2g} bands, and a significant localization of electrons at the Fermi surface [Fig. 3(a)]. Our calculations also show that the total $3d$ electron population within the Mn sphere in GaN:Mn is around 4.59, and does not depend on the Mn concentration, i.e., the atomic configuration of Mn is compatible with both $3d^4$ and $3d^5$.

Many of these features are observed in the electronic structure of the ferromagnetic GaAs:Mn with 3.125% of Mn [Fig. 1(b)]. The exchange splitting of Mn states is much larger than the crystal field one (3.4 eV vs 0.4 eV), as in the

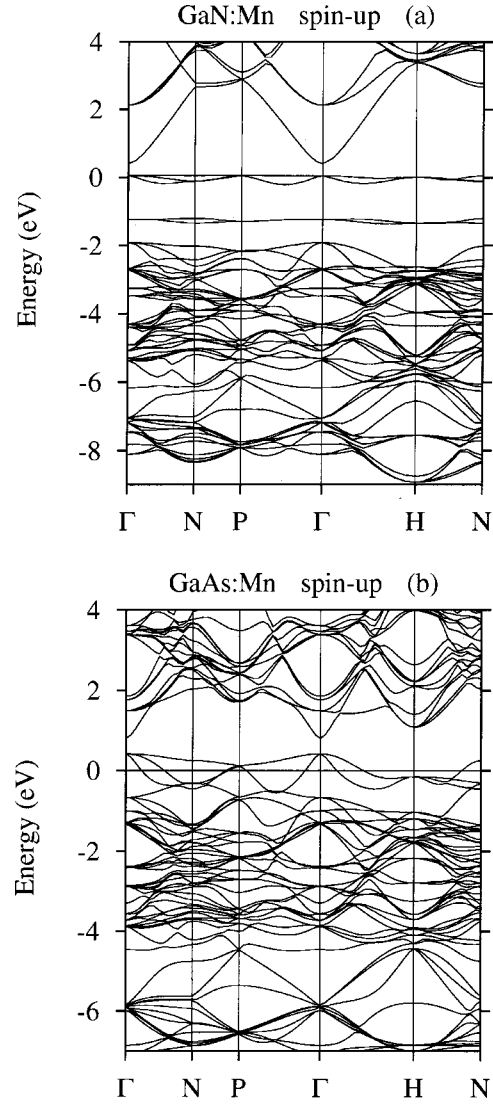


FIG. 2. Ferromagnetic energy bands of GaN:Mn (a) and GaAs:Mn (b) at 3.125% of Mn in the spin-up channel. The Fermi energy is depicted by the horizontal line at zero energy.

TABLE I. Magnetic moments in GaN:Mn. 1NN means a first-nearest neighbor to the Mn atom.

% of Mn	1.56	3.125	6.25	12.5
Ferromagnetic phase				
$M^{\text{total}}(\mu_B/\text{cell})$	4	8	8	8
$m^{\text{Mn}}(\mu_B)$	3.322	3.341	3.390	3.376
$m^{\text{N}(1\text{NN})}(\mu_B)$	0.044	0.039	0.038	0.043
$m^{\text{Ga}(1\text{NN})}(\mu_B)$	0.007	0.008	0.016	0.032
Antiferromagnetic phase				
$M^{\text{total}}(\mu_B/\text{cell})$	0	0	0	0
$m^{\text{Mn}(\uparrow, \downarrow)}(\mu_B)$	± 3.329	± 3.283	± 3.345	± 3.345
$m^{\text{N}(1\text{NN})}(\mu_B)$	± 0.043	± 0.035	± 0.038	± 0.038
$m^{\text{Ga}(1\text{NN})}(\mu_B)$	± 0.007	± 0.015	0	0

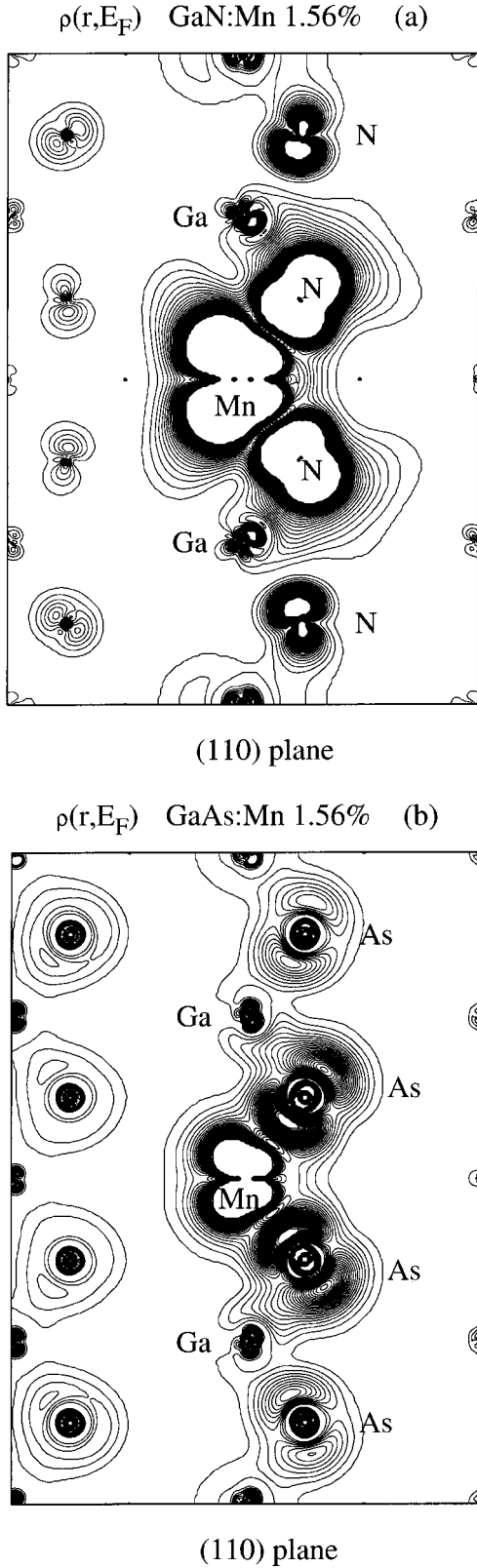


FIG. 3. (110)-plane charge density in hybridized states near the Fermi energy (0.2-eV energy window) for ferromagnetic GaN:Mn (a) and GaAs:Mn (b) (1.56% of Mn). Successive contours differ by $\rho_{n+1} - \rho_n = 0.001 e/\text{\AA}^3$.

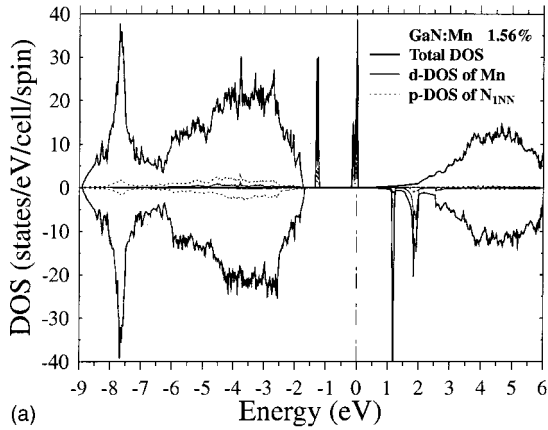
TABLE II. Magnetic moments in GaAs:Mn.

% of Mn	1.56	3.125	6.25	12.5
Ferromagnetic phase				
$M^{\text{total}}(\mu_B/\text{cell})$	4	8	8	7.713
$m^{\text{Mn}}(\mu_B)$	3.715	3.632	3.637	3.582
$m^{\text{As}(1\text{NN})}(\mu_B)$	-0.011	-0.015	-0.010	-0.029
$m^{\text{Ga}(1\text{NN})}(\mu_B)$	0.011	0.013	0.026	0.045
Antiferromagnetic phase				
$M^{\text{total}}(\mu_B/\text{cell})$	0	0	0	0
$m^{\text{Mn}}(\uparrow, \downarrow)(\mu_B)$	± 3.621	± 3.388	± 3.416	± 3.416
$m^{\text{As}(1\text{NN})}(\mu_B)$	∓ 0.006	∓ 0.046	∓ 0.049	∓ 0.049
$m^{\text{Ga}(1\text{NN})}(\mu_B)$	± 0.013	± 0.017	± 0.017	0

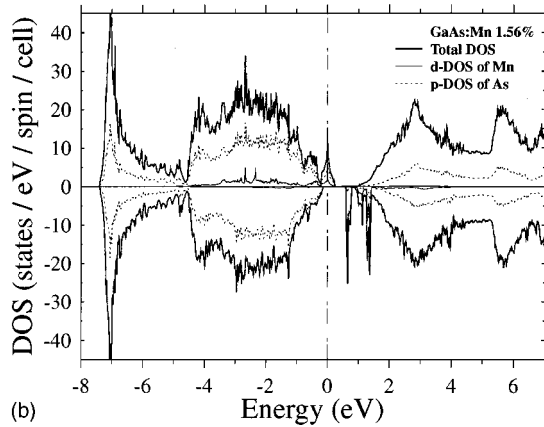
case of GaN:Mn. Due to this, GaAs:Mn is half-metallic, with the Fermi level inside the spin-up t_{2g} manifold. The total magnetic moment is also equal to $8\mu_B$ and localized at Mn (Table II). The most important difference between two materials concerns the energy position and localization of impurity spin-up states. In GaAs:Mn, the t_{2g} band of Mn lies just slightly above the top of the VB, while the e_g band falls into the VB and is barely distinguished there [Fig. 2(b)]. Both bands, especially e_g 's, are substantially hybridized with the electronic states of the VB. This leads to longer tails of Mn spin-up orbitals and less localized electronic states at the Fermi level compared to GaN:Mn [Fig. 3(b)]. In GaAs:Mn, the atomic configuration is compatible with both $3d^5$ and $3d^6$, as follows from our analysis of the total $3d$ population within the Mn sphere. This $3d$ population is equal to 5.17, and practically does not depend on the Mn concentration. This result is in good agreement with the results obtained in Refs. 13 and 15.

The difference in the energy positions of impurity bands between GaN:Mn and GaAs:Mn is preserved at all concentrations of Mn (Figs. 4 and 5). Evidently, this is due to a smaller size of N atoms compared to As atoms. This difference in sizes leads to a smaller lattice constant of GaN ($8.504a_B$ vs $10.677a_B$), to an additional compression of Mn orbitals and to a higher kinetic energy of the Mn states in GaN. The comparison of DOS's shows that ΔE_{xc} and ΔE_{cryst} depend weakly on the Mn concentration. The effect of concentration manifests itself mostly in the widths of Mn bands. As a result, the impurity states near the Fermi level remain perfectly spin polarized and M^{total} is equal to $8\mu_B$ in both materials at all concentrations, excluding the GaAs:Mn with 12.5% of Mn. The exception is due to the energy overlapping of the spin-up t_{2g} bands and spin-down e_g bands, which become too wide as the Mn doping grows. The stability of a 100% spin polarization of electronic states near the Fermi energy all over the concentration region shows a high validity of this result, which will hardly change even if electronic correlations in Mn bands are considered more thoroughly.

The spatial distribution of impurity states is intimately linked with the value of magnetic moments on different atoms. Tables I and II show that the main contribution to M^{total} comes from Mn atoms. In GaAs:Mn, this main magnetic



(a)

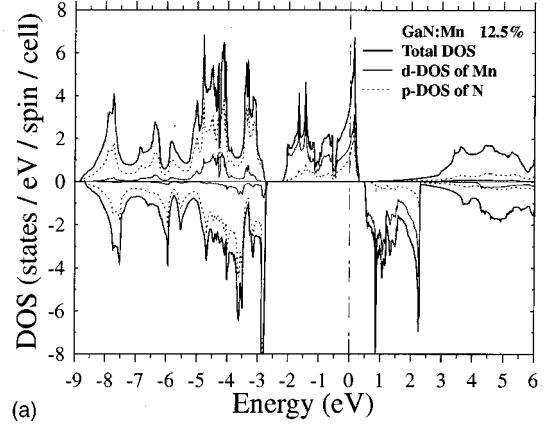


(b)

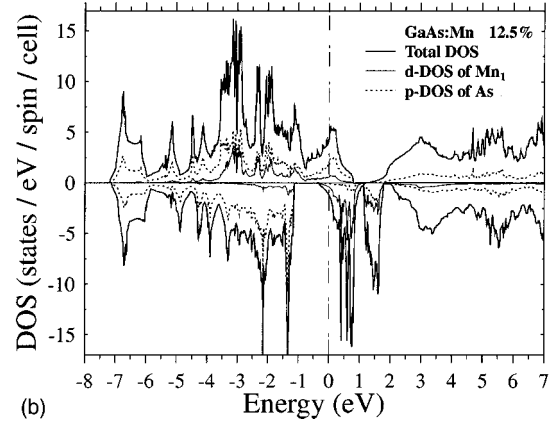
FIG. 4. Same as Fig. 1, but for 1.56% of Mn.

moment is screened by antiparallel moments on the nearest As atoms of Mn. This behavior is typical of the Ruderman-Kittel-Kasuya-Yoshida model, which describes a magnetic moment embedded in uniform electron gas. In GaN:Mn, magnetic moments of all atoms are parallel. This may be interpreted as a tunneling of spin-up impurity states to neighboring atoms. In this way, parallel or antiparallel orientation of magnetic moments on the atoms nearest to Mn may be considered as a signal that impurity states are either localized or strongly hybridized with the VB. It should be noted that the values of Mn magnetic moments practically do not depend on the Mn concentration. For GaAs:Mn, these results are well supported by experimental data that give a negative contribution of As atoms to the total magnetic moment.²² It would be of interest also to perform similar magnetic circular dichroism experiments for GaN:Mn and measure the orientation of magnetic moments on N.

To examine the stability of the FM state in GaN(As):Mn systems, we compared its total energy with the energy of PM and AFM states. The results presented in Table III show that the ferromagnetic state has a very large gain in energy of 0.4–0.5 eV per atom of Mn. This gain correlates well with a huge gain in one-electron energy (E_{bnd}) of 4–6 eV per atom of Mn, which comes from the energy lowering of magnetic electrons caused by exchange splitting and a much smaller cost produced by the redistribution of two electrons from the e_g band to the t_{2g} band:



(a)



(b)

FIG. 5. Same as Fig. 1, but for 12.5% of Mn.

$$E_{bnd}^{FM} - E_{bnd}^{PM} \approx -4\Delta E_{xc}/2 + 2\Delta E_{cryst}. \quad (1)$$

In Eq. (1) we neglected the widths of the e_g and t_{2g} bands and the difference in the exchange splitting of these bands. This simple estimation provides results that are in good agreement with the calculated band energy gains given in Table III. Competition between FM and AFM states is much stiffer and is due to the interaction of magnetic moments of Mn atoms spaced at considerable distances. This interaction must be weaker in GaN:Mn, where magnetic moments are strongly localized. As a result, the absolute value of energy

TABLE III. Total-energy differences (in eV/Mn) for several Mn concentrations in GaN:Mn and GaAs:Mn. Subscript *bnd* refers to the *one-electron* energy differences.

% of Mn	GaN:Mn			
	1.56	3.125	6.25	12.5
PM-FM	0.374	0.393	0.565	0.589
AFM-FM		0.023	0.047	0.021
(PM-FM) _{bnd}	3.921	4.013	3.561	2.422
% of Mn	GaAs:Mn			
	1.56	3.125	6.25	12.5
PM-FM	0.500	0.395	0.625	0.637
AFM-FM		0.088	0.039	0.052
(PM-FM) _{bnd}	6.076	6.198	5.094	4.936

gain between FM and AFM states should be smaller for GaN:Mn than for GaAs:Mn. The data given in Table III support this expectation, and show that the ferromagnetic state is preferable in both systems.

Weaker magnetic interaction of Mn magnetic moments in GaN:Mn may be considered as an indication of a lower Curie temperature of this material. However this conclusion is valid only in the case of homogeneous distribution of Mn atoms. The tendency toward the formation of the Mn_4N compound can result in an inhomogeneous distribution of Mn atoms in GaN:Mn. The effect of such an inhomogeneity will be very significant. For example, disposition of two Mn atoms on the nearest Ga sites will cause strong hybridization of their $3d$ orbitals and coupling of t_{2g} and e_g states in one combined band. These changes will delocalize impurity states and increase the magnetic interaction of Mn atoms. It is difficult, however, to estimate these effects in general, as inhomogeneity in the distribution of Mn atoms is a technology driven parameter, which may be individual for each experiment.

IV. KINETIC AND OPTICAL PROPERTIES

Electron velocity at the Fermi level is one of important kinetic characteristics of material which essentially affects carrier mobility. To give a first estimation of the velocity, we supposed that extra electrons of Mn (four electrons per Mn atom) form a perfectly spin-polarized free-electron gas, which is uniformly distributed in the supercell. For a 3.125% Mn concentration such a free-electron estimation provides $v_F(\text{GaN:Mn}) = 1.00 \times 10^8$ cm/s and $v_F(\text{GaAs:Mn}) = 0.81 \times 10^8$ cm/s. For comparison, in metallic Rb the Fermi velocity is also 0.81×10^8 cm/s.

Band calculation of the square-root averaged Fermi velocity (\bar{v}_F) was carried out by using the expression

$$\bar{v}_F^2 = \sum_{\lambda} \int d\mathbf{k} \delta[E_{\lambda}(\mathbf{k}) - E_F] \times [\nabla_{\mathbf{k}} E_{\lambda}(\mathbf{k}) / \hbar]^2 / \sum_{\lambda} \int d\mathbf{k} \delta[E_{\lambda}(\mathbf{k}) - E_F], \quad (2)$$

where $E_{\lambda}(\mathbf{k})$ is an electron energy in the λ th band and E_F is the Fermi energy. The calculation gave $v_F(\text{GaN:Mn}) = 0.20 \times 10^8$ cm/s and $v_F(\text{GaAs:Mn}) = 1.13 \times 10^8$ cm/s. That is, in GaN:Mn the value of \bar{v}_F is a mere $0.2v_F$, while in GaAs:Mn \bar{v}_F is even 1.4 times the free-electron value. This result well correlates with the band structure of GaN(As):Mn given in Fig. 2. The spin-up t_{2g} bands of GaN:Mn show a weak dispersion, which follows from a small overlapping of impurity orbitals of neighboring Mn atoms. The dispersion of the spin-up t_{2g} bands of GaAs:Mn near the Γ point is large and greatly repeats the dispersion of the VB near its top. This effect is due to a strong hybridization of Mn impurity states with the states of the VB. It is this hybridization that causes large dispersion in the spin-up impurity bands and increases $\bar{v}_F(\text{GaAs:Mn})$, as compared to its free-electron value.

These calculations were based on the band description of the electronic structure of GaN(As):Mn, which predicts half-metallicity for both materials. In a more careful description, which involves electronic correlations, the metallicity holds only until a t_{2g} bandwidth is larger than the energy cost caused by an electronic jump from one Mn atom to another. The metallic conductivity of GaAs:Mn was reported in Ref. 3, so the validity of the band description is a matter of fact for this material. This fact agrees with a significant width of the t_{2g} band of GaAs:Mn, which is due to its hybridization with the VB. In GaN:Mn, where the t_{2g} band is narrower, both descriptions look competitive. Inhomogeneity in the space distribution of Mn atoms decreases the localization of the t_{2g} states and increases the bandwidth, as discussed at the end of Sec. III. In this case, the band approach is quite justified and the band result for the Fermi velocity of GaN:Mn appears quite realistic.

An analysis of spin-up bands in GaN(As):Mn shows that impurity states may manifest themselves in certain features of optical spectra inside the gap region. These features produced by Mn provide an opportunity for experimental determination of the spin-up e_g - and t_{2g} band positions. To verify this idea, we carried out optical calculations of GaN(As):Mn with 3.125% of Mn. In these calculations, we used an extended LMTO basis, which additionally included the Mn $4f$ and N (As) $3d$ ($4d$) orbitals. As the splitting caused by spin-orbit coupling (SOC) is compared in value with the width of Mn bands and their distance from the top of the VB, SOC terms were added to an electron Hamiltonian. The scheme of optical calculations was the same as in our earlier work.²³ It involved a direct calculation of the imaginary part of the dielectric function $\text{Im} \varepsilon(\omega)$ and a calculation of $\text{Re} \varepsilon(\omega)$ with the Kramers-Kronig relation. Intraband transitions in the spin-up t_{2g} bands were described by the Drude contribution with the squared plasma frequency $\omega_p^2 = 4\pi e^2 N(E_F) \bar{v}_F^2 / m$, where $N(E_F)$ is the density of states at the Fermi level. The calculated $\varepsilon(\omega)$ was used then to find reflectivity $R(\omega)$.

The results of these calculations are presented in Fig. 6. In GaN:Mn, the most interesting feature is a peak of $\text{Im} \varepsilon(\omega)$ at $\hbar\omega = 1.25$ eV, which causes the maximum of $R(\omega)$ at the same energy. An analysis of the DOS and the band structure (Figs. 1 and 2) shows that most probably this is caused by the electronic transitions between the spin-up e_g and t_{2g} bands. Because of the $\Delta l = \pm 1$ selection rule, the contribution of Mn to the matrix elements of these transitions is zero. The nonzero contribution arises from the tails of impurity states situated at the atoms surrounding Mn. These overlapping tails give the only contribution to the matrix elements. A numerical experiment, where only $e_g \rightarrow t_{2g}$ transitions were taken into account, supported this analysis. It was found that these transitions contribute more than 95% to $\text{Im} \varepsilon(\omega)$ at $\hbar\omega \sim 1.25$ eV. In GaAs:Mn, this feature is shifted down in energy to 0.8 eV and significantly decreases in amplitude, because of strong hybridization of the spin-up e_g band with the VB. The maximum of $\text{Im} \varepsilon(\omega)$ at 0.35 eV is caused by transitions inside the spin-up t_{2g} band, as expected from the

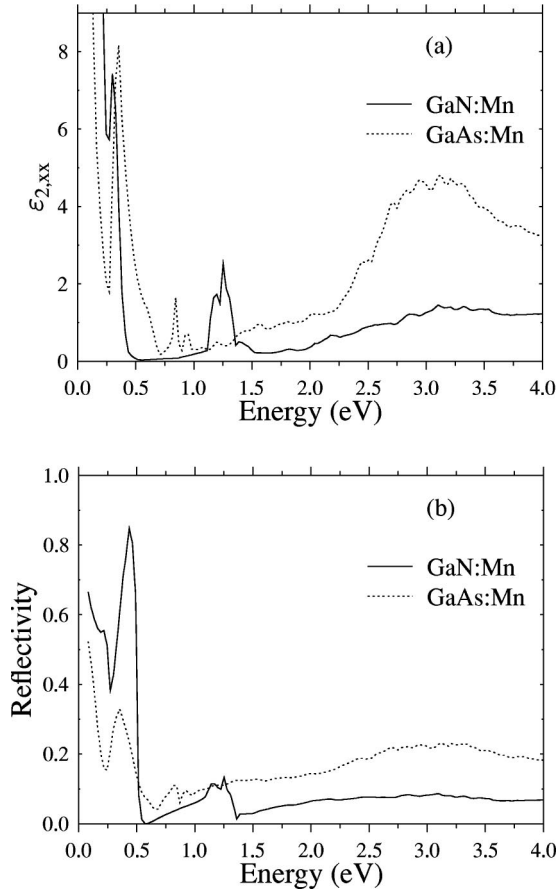


FIG. 6. Calculated imaginary part of the dielectric function $\epsilon_2(\omega)$ (a) and reflectivity $R(\omega)$ (b) for GaN:Mn (solid lines) and GaAs:Mn (dashed lines). The concentration of Mn is 3.125%.

band structure of GaAs:Mn (Fig. 2). This maximum results in the peak of $R(\omega)$ at 0.35 eV.

Summing up these results, we state that the sharp reflectivity edge at 0.47 eV and the peak of $R(\omega)$ at 1.25 eV, calculated in GaN:Mn, are clear manifestations of Mn

TABLE IV. Total-energy differences (in eV/Mn) and magnetic moments in ferromagnetic GaN:Mn codoped with Zn and O.

% of Mn	3.125	6.25	12.5
		Zn codoping	
PM-FM	0.213	0.257	0.283
		O codoping	
PM-FM	1.393	1.337	1.134
		Zn codoping	
$M^{\text{total}}(\mu_B/\text{cell})$	3	3	3
$m^{\text{Mn}}(\mu_B)$	2.836	2.813	2.802
$m^{\text{Zn}}(\mu_B)$	-0.016	-0.004	0.018
		O codoping	
$M^{\text{total}}(\mu_B/\text{cell})$	4.967	4.952	4.936
$m^{\text{Mn}}(\mu_B)$	3.961	3.963	3.976
$m^{\text{O}}(\mu_B)$	+0.060	+0.069	+0.096

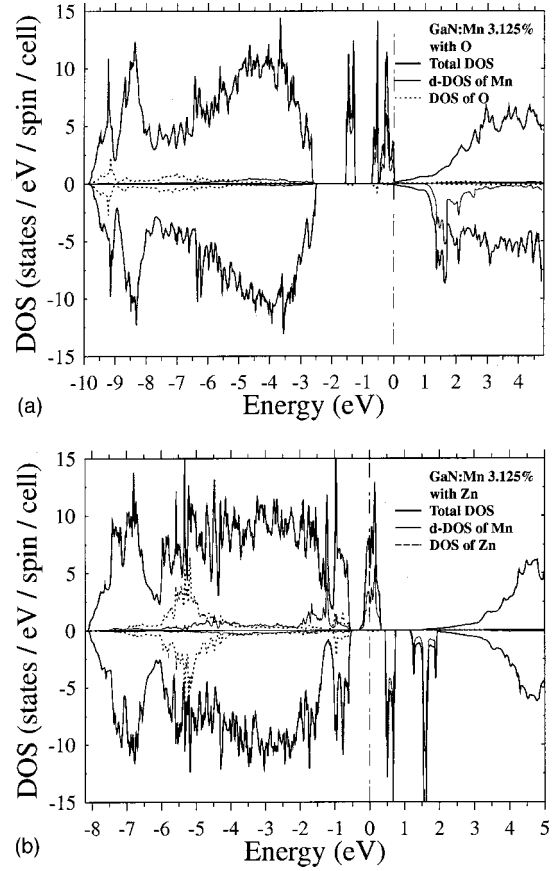


FIG. 7. Ferromagnetic DOS of GaN:Mn at 3.125% of Mn calculated for cases: (a) *n*-type codoping by oxygen and (b) *p*-type codoping by zinc. The total DOS is shown by the bold line. The thin line is the 3*d* DOS of Mn, and the dashed lines are the (*s*+*p*+*d*) DOS's of codopants [O (a) and Zn (b)]. The vertical dot-dashed line denotes the position of the Fermi level, which is set as the zero energy.

spin-up bands well separated from the top of the VB. In this way, measurements of the reflectivity can provide valuable information about impurity states in the GaN:Mn system.

V. EFFECT OF CODOPING ON FERROMAGNETIC PROPERTIES

In this section we consider the effect of co-doping on properties of the GaN:Mn system using both *p*- and *n*-type codopants, namely, zinc and oxygen. Calculations were made for ferromagnetic DMS's with Mn concentrations of 3.125%, 6.25%, and 12.5%. In the 64-atom cell, either Ga or N was replaced by zinc or oxygen, respectively. The calculated results are summarized in Table IV, which presents the total-energy gains and values of magnetic moments on the Mn and codoping sites. Figure 7 shows DOS's of GaN:Mn (3.125% of Mn) in the cases of O and Zn codoping. Our results show that the O codoping drastically enhances the gain of the FM state over the PM one. The magnetic moment of Mn almost reaches $4\mu_B$ (the maximum value for the Mn site in GaN:Mn). The spin-up Mn 3*d* bands become almost fully occupied, while spin-down 3*d* states remain empty and

merge with the CB. The oxygen states are highly hybridized with the VB, and the magnetic moment at the O site is parallel to the Mn moment. Most probably oxygen not only enhances ferromagnetism, but also causes a significant increase in the Curie temperature of GaN:Mn.

The effect of Zn codoping is completely different. The total energy gain (FM vs PM) decreases with the zinc codoping, in line with a smaller magnetic moment of Mn and the decrease of M^{total} to $3\mu_B$ (Table IV). Half-metallicity is preserved in the case of the Zn codoping. However, the e_g states of Mn are strongly hybridized with the VB and change its shape (Fig. 7). It is difficult, however, to predict the change of Curie temperature in case of the Zn codoping, as the decrease of M^{total} and the hybridization of Mn states work in opposite directions.

VI. CONCLUSIONS

We performed *ab initio* calculations of the electronic structure, magnetic, kinetic, and optical properties in uniformly superdoped GaN(As):Mn systems with the zinc-blende lattice. It was found that different energy positions of impurity Mn states relative to the top of the VB determine rather distinctive properties of GaN:Mn and GaAs:Mn. In GaN:Mn, impurity states are located deep inside the gap, strongly localized near Mn atoms and have low velocities at the Fermi level. The magnetic moments of all atoms are parallel and magnetic interaction of Mn atoms is short ranged. This leads to a small energy difference between the ferro and antiferromagnetic states of GaN:Mn. Conversely, in GaAs:Mn the $3d$ states of Mn are located near the top of the VB and are well hybridized with its electronic states. This results in a high Fermi velocity, which even exceeds free-electron estimation, and a rather long-range magnetic

interaction of Mn atoms partially screened by antiparallel orientation of magnetic moments at the nearest As atoms. These results allow us to consider GaN:Mn and GaAs:Mn as representatives of two different groups of DMS's.

Codoping by O and Zn atoms (n and p type) significantly changes the position of impurity bands and the properties of GaN:Mn. Our calculations yielded the following two important effects: (i) the large enhancement of ferromagnetism with the oxygen codoping, which may increase Curie temperature; and (ii) the delocalization of the e_g states of Mn with the zinc codoping. Inhomogeneous distribution of Mn atoms is another factor, that may strongly affect kinetic and magnetic properties of DMS's. The recent observation of Curie temperature $T_C \approx 940$ K in the wurtzite $\text{Ga}_{0.91}\text{Mn}_{0.09}$ prepared with ammonia⁷ shows that these technology-driven factors may be highly important for the properties of a DMS. Further experimental studies combined with focused theoretical analysis are highly desirable for a deeper insight into the nature of magnetism in superdoped GaN(As):Mn systems and its quantitative description.

ACKNOWLEDGMENTS

This work was supported by the JSPS Research for the Future Program in the Area of Atomic Scale Surfaces and Interface Dynamics (Japan), and by the CNRS-Grenoble (France). Computations have been performed at the Media Center of Osaka City University and partially at the CEA computer center in Grenoble. The authors are grateful to O. Jepsen for providing us with the TB-LMTO program. Two of us (E.K. and Yu. A.U.) acknowledge financial support from the Russian Fund of Basic Investigations (Grant No. 01-02-17432-a).

[†]Permanent address: General Physics Institute, Russian Academy of Sciences, Vavilov str. 38, Moscow, Russia.

*Corresponding author: Hiroshi Nakayama, Department of Applied Physics, Faculty of Engineering, Osaka City University, 3-3-138 Sugimoto, Sumiyoshi, Osaka 558-8585, Japan Phone: +81-6-6605-3088, Fax: +81-6-6605-3088. Email address: hiroshi@ap-physics.eng.osaka-cu.ac.jp

¹H. Ohno, J. Magn. Mater. **200**, 110 (1999).

²H. Ohno, Science **281**, 951 (1998).

³T. Dietl, H. Ohno, F. Matsukura, J. Cibert, and D. Ferrand, Science **287**, 1019 (2000).

⁴Y. Ohno, D. K. Young, B. Beschoten, F. Matsukura, H. Ohno, and D. D. Awschalom, Nature (London) **402**, 790 (1999).

⁵H. Nakayama, H. Ohta, and E. Kulatov, Thin Solid Films **395**, 230 (2001).

⁶H. Nakayama and E. Kulatov, invited lecture in *Proceedings of the Sixth International Symposium on Advanced Physical Fields (APF-6): Growth of Well-Defined Nanostructures*, edited by N. Koguchi (Tsukuba, Japan, 2001), p. 28.

⁷S. Sonoda, S. Shimizu, T. Sasaki, Y. Yamamoto, and H. Hori, <http://xxx.lanl.gov/abs/cond-mat/0108159> (unpublished).

⁸M. L. Reed, N. A. El-Masry, H. H. Stadelmaier, M. K. Rittums, M. J. Reed, C. A. Parker, J. C. Roberts, and S. M. Bedair, Appl. Phys. Lett. **79**, 3473 (2001).

⁹E. Kulatov, H. Nakayama, and H. Ohta (unpublished).

¹⁰M. Shirai, T. Ogawa, I. Kitagawa, and N. Suzuki, J. Magn. Mater. **177–181**, 1383 (1998).

¹¹T. Ogawa, M. Shirai, N. Suzuki, and I. Kitagawa, J. Magn. Mater. **196–197**, 428 (1999).

¹²M. Shirai, Photonics Spectra **10**, 143 (2001). We are grateful to Dr. Shirai for showing us his band structure results prior to publication.

¹³S. Sanvito, P. Ordejon, and N. A. Hill, Phys. Rev. B **63**, 165206 (2001); S. Sanvito and N. A. Hill, Appl. Phys. Lett. **78**, 3493 (2001).

¹⁴Mark van Schilfgaarde and O. N. Mryasov, Phys. Rev. B **63**, 233205 (2001).

¹⁵Yu-Jun Zhao, W. T. Geng, K. T. Park, and A. J. Freeman, Phys. Rev. B **64**, 035207 (2001).

¹⁶T. C. Schulthess and W. H. Butler, J. Appl. Phys. **89**, 7021 (2001).

¹⁷M. Jain, L. Kronik, J. R. Chelikowsky, and V. V. Godlevsky, Phys. Rev. B **64**, 245205 (2001).

¹⁸O. K. Andersen and O. Jepsen, Phys. Rev. Lett. **53**, 2571 (1984); O. K. Andersen, O. Jepsen, and D. Glotzel, in *Highlights of Condensed-Matter Theory*, edited by F. Bassani, F. Fumi, and M. P. Tosi (North-Holland, New York, 1985).

- ¹⁹S. Yu. Savrasov, Phys. Rev. B **54**, 16 470 (1996).
- ²⁰P. Bloechl, O. Jepsen, and O. K. Andersen, Phys. Rev. B **49**, 16 223 (1994).
- ²¹U. von Barth and L. Hedin, J. Phys. C **5**, 1629 (1972).
- ²²B. Beschoten, P. A. Crowell, I. Malajovich, and D. D. Awschalom, Phys. Rev. Lett. **83**, 3073 (1999).
- ²³Yu. A. Uspenskii, E. T. Kulatov, and S. V. Halilov, Phys. Rev. B **54**, 474 (1996).